A&A 451, 409–416 (2006)
DOI: 10.1051/0004-6361:20054705

Astronomy & Astrophysics

The VIMOS-VLT Deep Survey

Luminosity dependence of clustering at $z \simeq 1$⋆

A. Pollo[1,2,15], L. Guzzo[2], O. Le Fèvre[1], B. Meneux[1], A. Cappi[3], P. Franzetti[4], A. Iovino[2], H. J. McCracken[5,6], C. Marinoni[7,1], G. Zamorani[3], D. Bottini[4], B. Garilli[4], V. Le Brun[1], D. Maccagni[4], J. P. Picat[8], R. Scaramella[9], M. Scodeggio[4], L. Tresse[1], G. Vettolani[10], A. Zanichelli[10], C. Adami[1], S. Arnouts[1], S. Bardelli[3], M. Bolzonella[14], S. Charlot[5], P. Ciliegi[3], T. Contini[8], S. Foucaud[12], I. Gavignaud[8,13], O. Ilbert[14], B. Marano[14], A. Mazure[1], R. Merighi[3], S. Paltani[19,20], R. Pellò[8], L. Pozzetti[3], M. Radovich[17], E. Zucca[3], M. Bondi[10], A. Bongiorno[14], G. Busarello[17], O. Cucciati[2,18], L. Gregorini[10], F. Lamareille[8], G. Mathez[8], Y. Mellier[5,6], P. Merluzzi[17], V. Ripepi[17], and D. Rizzo[16]

(Affiliations can be found after the references)

Received 16 December 2005 / Accepted 16 January 2006

ABSTRACT

We investigate the dependence of galaxy clustering on the galaxy intrinsic luminosity at high redshift, using the data from the First Epoch VIMOS-VLT Deep Survey (VVDS). The size (6530 galaxies) and depth ($I_{AB} < 24$) of the survey allows us to measure the projected two-point correlation function of galaxies, $w_p(r_p)$, for a set of volume-limited samples up to an effective redshift $\langle z \rangle = 0.9$ and median absolute magnitude $-19.6 < M_B < -21.3$. Fitting $w_p(r_p)$ with a single power-law model for the real-space correlation function $\xi(r) = (r/r_0)^{-\gamma}$, we measure the relationship of the correlation length r_0 and the slope γ with the sample median luminosity for the first time at such high redshift. Values from our lower-redshift samples ($0.1 < z < 0.5$) are fully consistent with the trend observed by larger local surveys. In our high redshift sample ($0.5 < z < 1.2$), we find that the clustering strength suddenly rises around M_B^*, apparently with a sharper inflection than at low redshifts. Galaxies in the faintest sample ($\langle M_B \rangle = -19.6$) have a correlation length $r_0 = 2.7^{+0.3}_{-0.3}\ h^{-1}$ Mpc, compared to $r_0 = 5.0^{+1.5}_{-1.6}\ h^{-1}$ Mpc at $\langle M_B \rangle = -21.3$. The slope of the correlation function is observed to correspondingly steepen significantly from $\gamma = 1.6^{+0.1}_{-0.1}$ to $\gamma = 2.4^{+0.4}_{-0.2}$. This is not observed either by large local surveys or in our lower-redshift samples and seems to imply a significant change in the way luminous galaxies trace dark-matter halos at $z \sim 1$ with respect to $z \sim 0$. At our effective median redshift $z \simeq 0.9$ this corresponds to a strong difference of the relative bias, from $b/b* < 0.7$ for galaxies with $L < L*$ to $b/b* \simeq 1.4$ for galaxies with $L > L*$.

Key words. cosmology: large scale structure of Universe – cosmology: observations – methods: statistical – galaxies: evolution

1. Introduction

At the current epoch, luminous galaxies tend to be more clustered than faint ones (Davis et al. 1988; Hamilton 1988; Iovino et al. 1993; Maurogordato & Lachieze-Rey 1991; Benoist et al. 1996; Willmer et al. 1998; Guzzo et al. 2000; Norberg et al. 2001, 2002; Zehavi et al. 2005), with the difference becoming remarkable above the characteristic luminosity L_* of the Schechter luminosity function. This effect is in general agreement with predictions from hierarchical models of galaxy formation (White et al. 1987; Valls-Gabaud et al. 1989; Kauffmann et al. 1997; Benson et al. 2001), in which bright galaxies are expected to occupy more massive dark matter haloes than fainter ones and these haloes are more strongly clustered than the overall distribution of dark matter (Kaiser 1984; Mo & White 1996; Sheth & Tormen 1999). If this is the case, the difference in clustering between faint and bright galaxies should become even more evident at high redshifts, where galaxy formation is supposed to be more confined to the highest peaks of the density field.

Understanding the relationship between galaxies and dark matter halos is one of the most difficult challenges of the theory in predicting the observed clustering of galaxies. Over the last few years, *halo occupation models* have provided this connection in a phenomenological way, allowing one, e.g., to explain the detailed shape of the galaxy two-point correlation function (Zehavi et al. 2004; but see also Guzzo et al. 1991). In these models, a statistically motivated recipe to describe galaxy formation determines the halo occupation distribution (HOD), specifying the probability $P(N|M)$ that a halo of virial mass M contains N galaxies of a given type, together with any spatial and velocity biases of galaxies (Kauffmann et al. 1997;

⋆ Based on data obtained with the European Southern Observatory Very Large Telescope, Paranal, Chile, program 070.A-9007(A), and on data obtained at the Canada-France-Hawaii Telescope, operated by the CNRS of France, CNRC in Canada and the University of Hawaii.

Benson et al. 2001; Berlind et al. 2003; Kravtsov et al. 2004). This term (known as the *one-halo component* of the correlation function) governs the behaviour of galaxy correlations on small (<2 h^{-1} Mpc) scales, while at larger separations galaxy correlations are dominated by the gravitational clustering of virialized dark matter halos (the *two-halo component*), with essentially no dependence on the more complex physics of the sub-dominant baryonic component. Given cosmological parameters and a specified HOD, therefore, one can calculate any galaxy clustering statistic, on any scale (e.g., Abazajian et al. 2005), either by populating the halos from an N-body simulation (e.g., Jing et al. 1998, 2002) or via analytical prescriptions (e.g., Peacock & Smith 2000; Seljak 2000; Marinoni et al. 2002; Cooray & Sheth 2002; van den Bosch et al. 2003). On the other hand, as it has been shown (Sheth & Tormen 2004; Gao et al. 2005; Harker et al. 2005), there seems to exist a clear relationship between halo formation properties and halo clustering properties, which indicates that current HOD models may describe galaxy clustering at best approximately. Thus, observations of the relative clustering of galaxies with different intrinsic luminosities provide crucial constraints on HOD models.

The detailed luminosity dependence of clustering so far has been difficult to establish because of the limited dynamic range in luminosity for even the largest local galaxy redshift surveys (e.g. Norberg et al. 2001). It is even more problematic to study this effect at redshifts significantly different to zero. High redshift samples have been too small to allow subdivision into luminosity classes. An additional complication relates to evolution of the overall luminosity function: galaxies become brighter on average going back in time, thus comparison of high-redshift measurements to local values requires accurate knowledge of the evolution of the global luminosity function.

The VIMOS-VLT Deep Survey (VVDS) provides us with unique information to address these issues in detail. A first investigation of how the non-linear bias between galaxy and matter evolves with redshift for different luminosity classes has been presented in Marinoni et al. (2005). An analysis of the evolution of clustering of galaxies has been presented in Le Fèvre et al. (2005a), and the evolution of the dependence of clustering on spectral types has been discussed by Meneux et al. (2005). In this paper we use the same VVDS first-epoch data to measure in more detail the dependence of galaxy clustering on luminosity at $\langle z \rangle \simeq 0.9$, and compare it to local values from 2dFGRS and SDSS. We describe the VVDS catalog and the construction of volume limited samples in Sect. 2. Section 3 presents the methods to estimate and retrieve the best-fit parameters for the real-space correlation function. We present our results on the projected correlation function in Sect. 4, while the comparison to existing local surveys, together with a discussion of the results is given in Sect. 5.

Throughout this paper we use a Concordance Cosmology with $\Omega_{\rm m} = 0.3$ and $\Omega_\Lambda = 0.7$. The Hubble constant is normally parameterised via $h = H_0/100$ to ease comparison with previous works, while a value $H_0 = 70$ km s^{-1} Mpc^{-1} is used when computing absolute magnitudes. All correlation length values are quoted in comoving coordinates.

2. The data

2.1. The VVDS

The VIMOS-VLT Deep Survey (VVDS, Le Fèvre et al. 2005b) studies the evolution of galaxies and the large scale structure of the Universe to $z \sim 2$ and higher. The VVDS spectroscopic survey is performed with the VIMOS multi-object spectrograph at the European Southern Observatory Very Large Telescope (Le Fèvre et al. 2003) and complemented with multi-color BVRI imaging data obtained at the CFHT telescope (McCracken et al. 2003; Le Fèvre et al. 2004). The first-epoch VVDS data consist of more than 11 000 spectra obtained in two VVDS-Deep fields, covering 0.61 square degrees.

For this analysis, we use the data from the F02 "Deep" field, which is a purely magnitude limited survey to $I_{AB} = 24$ currently covering an area of 0.49 square degrees. Considering only galaxies with secure (>80% confidence) redshifts, this sample includes 6530 galaxies. Details about observations, data reduction, redshift measurement and quality assessment can be found in Le Fèvre et al. (2005b).

2.2. Luminosity-limited sub-samples

To measure the dependence of clustering on galaxy luminosity, we select two redshift slices to isolate comparable intervals of cosmic time. By choosing the intervals $z \in [0.1, 0.5]$ and $z \in [0.5, 1.2]$, we obtain two samples covering approximately 3.5 Gy of proper time, in the adopted cosmology. The high-redshift slice is compared to the low-redshift sample and to local samples like the 2dF Galaxy Redshift Survey (2dFGRS) and the Sloan Digital Sky Survey (SDSS). The low-redshift sample is also directly compared to existing local estimates, although the small volume and larger redshift limit do not allow a one-to-one match. Within each slice, we build a series of volume-limited (where statistically possible) or quasi-volume-limited sub-samples chosen to contain a statistically reasonable number of galaxies.

Absolute magnitudes for VVDS galaxies have been estimated by computing the appropriate K-correction via a SED fitting technique to the observed multi-band photometry (see Ilbert et al. 2005; and Franzetti et al. 2005, for details) and to ease comparison to previous work are reported here in the VEGA system.

Due to the apparent magnitude limit of the survey, as shown in Fig. 1, within the high-redshift slice a true volume-limited sample can be defined only for $M_B \lesssim -19.5$. Conversely, in the low-redshift slice we can define volume-limited sub-samples for $M_B \lesssim -17$. Because of the smaller volume probed we do not have a large number of bright galaxies in this latter sample. Therefore, as seen from Fig. 1, we cannot expect statistically sound measurements for galaxies closer than $z \sim 0.5$ with $M_B \lesssim -19.5$. All details on the selected VVDS sub-samples are listed in Tables 1 and 2. For each sub-sample, the columns give its absolute magnitude limit in the B band (1); its median M_B magnitude (2); the Schechter characteristic magnitude in that redshift range (3); the difference between the median and characteristic magnitudes (4); number of galaxies (5); median

Table 1. Properties of the VVDS luminosity sub-samples in the range $0.1 < z < 0.5$.

M_B range	$M_B^{\rm median}$	M_B^*	$M_B^{\rm med} - M_B^*$	$N_{\rm gal}$	$z_{\rm median}$	r_0	γ
<−16	–17.99	–19.97	1.98	1330	0.332	$2.55^{+0.54}_{-0.54}$	$1.69^{+0.14}_{-0.17}$
Volume limited:							
<−17.0	–18.30	–19.97	1.67	1089	0.363	$2.97^{+0.54}_{-0.46}$	$1.72^{+0.16}_{-0.12}$
<−17.5	–18.53	–19.97	1.44	883	0.373	$3.17^{+0.62}_{-0.62}$	$1.66^{+0.14}_{-0.11}$
<−18.0	–18.98	–19.97	0.99	658	0.381	$3.25^{+0.90}_{-0.92}$	$1.72^{+0.22}_{-0.18}$
<−18.5	–19.34	–19.97	0.63	475	0.388	$3.47^{+0.90}_{-0.90}$	$1.83^{+0.21}_{-0.20}$
<−19.0	–19.70	–19.97	0.27	318	0.381	$4.25^{+1.34}_{-1.54}$	$1.70^{+0.27}_{-0.26}$
<−19.5	–20.00	–19.97	–0.03	201	0.391	$3.65^{+2.26}_{-5.26}$	$1.50^{+0.51}_{-0.40}$

Table 2. As Table 1, but for $0.5 < z < 1.2$.

M_B range	$M_B^{\rm median}$	M_B^*	$M_B^{\rm med} - M_B^*$	$N_{\rm gal}$	$z_{\rm median}$	r_0	γ
<−17	–19.65	–20.76	1.11	4283	0.808	$2.75^{+0.27}_{-0.27}$	$1.59^{+0.09}_{-0.07}$
<−18.5	–19.80	–20.76	0.96	3736	0.856	$2.89^{+0.27}_{-0.27}$	$1.54^{+0.08}_{-0.07}$
<−19	–19.96	–20.76	0.80	3272	0.882	$2.95^{+0.33}_{-0.35}$	$1.52^{+0.09}_{-0.08}$
Volume limited:							
<−19.5	–20.23	–20.76	0.53	2407	0.899	$2.93^{+0.33}_{-0.35}$	$1.59^{+0.12}_{-0.09}$
<−20	–20.58	–20.76	0.18	1530	0.914	$3.47^{+0.46}_{-0.43}$	$1.84^{+0.14}_{-0.12}$
<−20.5	–20.92	–20.76	–0.16	865	0.913	$4.77^{+0.61}_{-0.61}$	$2.00^{+0.15}_{-0.12}$
<−21	–21.30	–20.76	–0.54	368	0.920	$5.01^{+1.47}_{-1.65}$	$2.38^{+0.36}_{-0.21}$

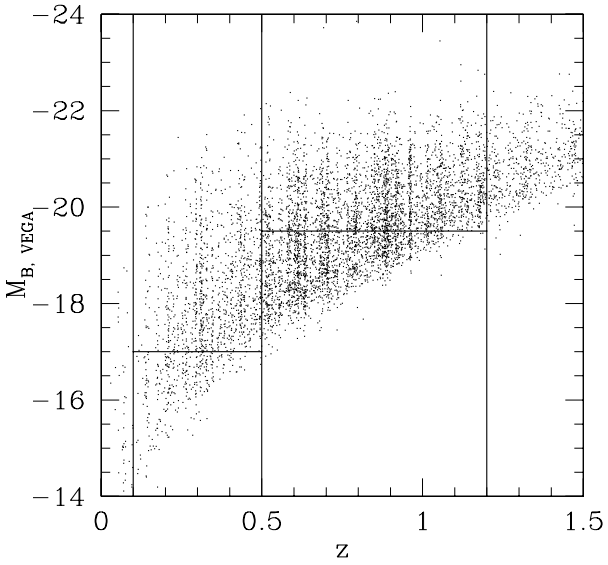

Fig. 1. Distribution of magnitudes of VVDS galaxies with redshift. Solid vertical lines show the boundaries of our two redshift slices. Solid horizontal lines show from which magnitudes ($M_B \sim 19.5$) our sub-samples are volume limited.

redshift (6); measured correlation length and the slope of the correlation function (7 and 8).

In the following sections we use – at different redshifts – the characteristic magnitude of the Schechter luminosity function in the B band, M_B^*, as a reference value. Normalizing our median absolute magnitude values at each redshift to the corresponding value of M_B^* provides a way to take into account the mean brightening of galaxies due to evolution, when comparing samples at different epochs. The values of M_B^* at each redshift are those estimated from these same data by Ilbert et al. (2005) in the AB system, converted here into the VEGA scale.

3. Estimating the real-space correlation function

We summarize here the methods applied to derive the real-space correlation function and its parameters, described extensively in Pollo et al. (2005). The galaxy real-space correlation length r_0 and slope γ from the VVDS-F02 data are measured from the projection of the redshift-space correlation function $\xi(r_{\rm p}, \pi)$, estimated using the Landy & Szalay (1993) estimator,

$$\xi(r_{\rm p},\pi) = \frac{N_{\rm R}(N_{\rm R}-1)}{N_{\rm G}(N_{\rm G}-1)}\frac{GG(r_{\rm p},\pi)}{RR(r_{\rm p},\pi)} - \frac{N_{\rm R}-1}{N_{\rm G}}\frac{GR(r_{\rm p},\pi)}{RR(r_{\rm p},\pi)} + 1, \quad (1)$$

where $N_{\rm G}$ and $N_{\rm R}$ are the total numbers of objects in the galaxy sample and in a catalog of random points distributed within the same survey volume and with the same redshift distribution and angular selection biases; $GG(r_{\rm p}, \pi)$ is the number of independent galaxy-galaxy pairs with separation perpendicular to the line of sight between π and $\pi + d\pi$ and separation parallel to the line of sight between $r_{\rm p}$ and $r_{\rm p} + {\rm d}r_{\rm p}$; $RR(r_{\rm p}, \pi)$ is the number of independent random-random pairs within the same interval of separations and $GR(r_{\rm p}, \pi)$ represents the number of galaxy-random pairs. A total of ∼40 000 random points has been used in each computation.

To derive the real-space correlation function and avoid the effect of peculiar velocities which distort the redshift space statistics, we integrate $\xi(r_{\rm p}, \pi)$ along the line of sight (see

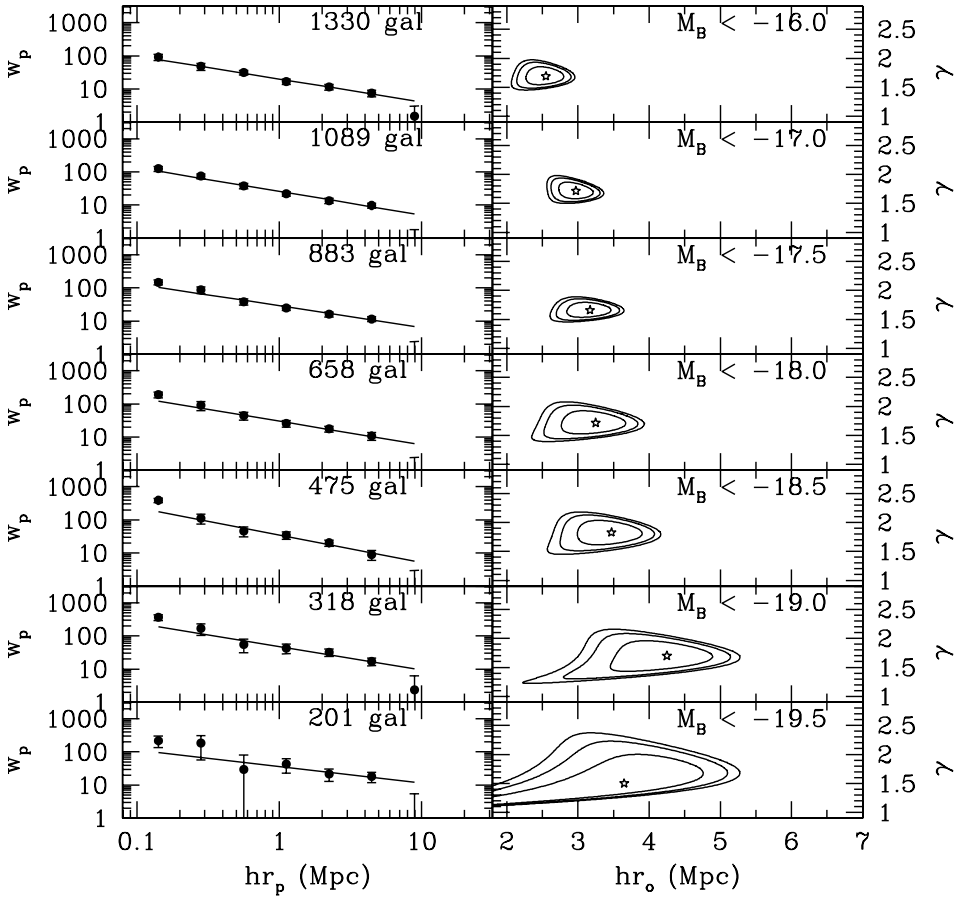

Fig. 2. Projected correlation functions $w_{\rm p}(r_{\rm p})$ and the associated r_0 and γ error countours for the seven volume limited catalogs at $z \leq 0.5$.

Davis & Peebles 1983), computing the projected correlation function,

$$w_{\rm p}(r_{\rm p}) \equiv 2\int_0^\infty \xi(r_{\rm p},\pi){\rm d}\pi = 2\int_0^\infty \xi\left[(r_{\rm p}^2+y^2)^{1/2}\right]{\rm d}y, \quad (2)$$

where ξ is the real space two-point correlation function evaluated at the specific separation $r = \sqrt{r_{\rm p}^2+y^2}$. In practice the upper integration limit has to be chosen finite, to avoid adding noise to the result. After a set of experiments we chose its optimal value as 20 h^{-1} Mpc. If $\xi(r)$ is well described by a power law, $\xi(r) = (r/r_0)^{-\gamma}$, the integral can be computed analytically, giving

$$w_{\rm p}(r_{\rm p}) = r_{\rm p}\left(\frac{r_0}{r_{\rm p}}\right)^\gamma \frac{\Gamma\left(\frac{1}{2}\right)\Gamma\left(\frac{\gamma-1}{2}\right)}{\Gamma\left(\frac{\gamma}{2}\right)}, \quad (3)$$

where Γ is Euler's Gamma function. Fitting $w_{\rm p}(r_{\rm p})$ for separations <10 h^{-1} Mpc using the procedure described in detail in Pollo et al. (2005) provides a best-fitting value of r_0 and γ for each volume-limited sub-sample.

The estimate of errors has been performed primarily using a bootstrap resampling of the data. However, our detailed error analysis in Pollo et al. (2005), based on 50 VVDS mock surveys from the GalICS simulations (Blaizot et al. 2005), indicates that bootstrap errors tend to be an underestimate of the true ensemble errors. The difficulty we encounter is that luminosity-selected sub-samples of our mock surveys do not show the same properties, in terms both of total numbers and scaling of the intrinsic clustering with luminosity, as the real VVDS. We have no guarantee, therefore, that for this specific application the variance among the mock samples represent a realistic estimate of the errors in the real data. For this reason, we have decided here to estimate error bars on $w_{\rm p}(r_{\rm p})$ using the bootstrap technique, but correct these empirically to include the contribution of cosmic variance. An average value for this correction has been estimated from the direct comparison of the errors computed in both ways for 50 whole mock samples (Meneux 2005; Pollo et al. 2005). The overall mean effect is to increase the size of the error bars on $w_{\rm p}$ by a factor of ∼2 for the low-redshift samples, and by a factor of ∼1.3 for the high-redshift samples. We applied this correction to all our bootstrap estimates of $w_{\rm p}(r_{\rm p})$. We have checked that our conclusions are robust to the details of this correction: even doubling the error bars in both redshift ranges, the trends in the values of correlation length and slope that we find at $z \sim 1$ do not change and remain significant.

4. Results

Figures 2 and 3 show the results of the power-law fits of the projected correlation functions $w_{\rm p}(r_{\rm p})$ and the corresponding r_0 and γ error contours, for the low- and high-redshift samples.

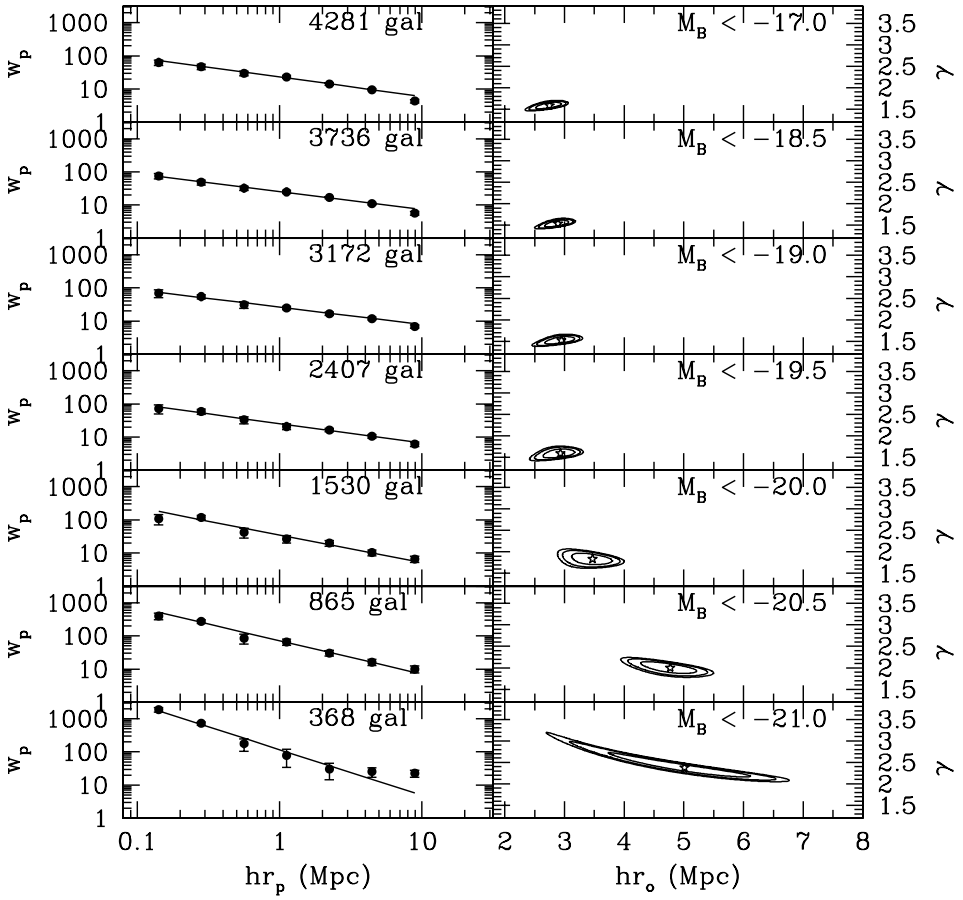

Fig. 3. Projected correlation functions $w_{\rm p}(r_{\rm p})$ and the associated r_0 and γ error countours for the seven high-redshift ($0.5 < z \leq 1.2$) samples.

The fitting has been performed taking into account the full covariance matrix of the data, as described in Pollo et al. (2005).

4.1. The correlation length r_0

A comparison of Figs. 2 and 3 shows qualitatively that for the high-redshift samples both the correlation length and the slope of the correlation function change with the sample luminosity. Note that we do not perform here any analysis of the detailed shape of $w_{\rm p}(r_{\rm p})$, its evolution and its implications for halo occupation models, but limit ourselves to the simple and robust fit of $w_{\rm p}(r_{\rm p})$ with a single power law.

In the left panel of Fig. 4 we compare our measurements of r_0 from the low-redshift VVDS samples to the similar measurements from the 2dFGRS (Norberg et al. 2001) and the SDSS (Zehavi et al. 2005). A one-to-one comparison is not possible, since the large size of local surveys allowed for the measurements in a series of disjoint volume-limited surveys with small magnitude intervals, i.e. $L1 \leq L \leq L2$, with $L1$ and $L2$ being their limiting luminosities. In our case we are forced to use integral measurements, i.e. samples with $L \leq L2$. Still, different sub-samples are dominated by galaxies with a specific characteristic luminosity that we characterize by computing the median absolute magnitude within each sample (reported in Tables 1 and 2). In addition, given the smaller volume of our low-redshift samples, it is clear that rare luminous objects will be under-represented. Finally, our low-redshift samples extend to $z = 0.5$ and thus may be regarded as a subsequent redshift bin after 2dFGRS and SDSS. Considering these intrinsic limitations , the overall trend is consistent with that observed by 2dFGRS and SDSS, although our measurements are systematically lower.

With this consistency in mind we analyze our VVDS high-redshift ($z \simeq 0.9$) samples and compare it to the local values from 2dFGRS and SDSS. This is done in the right panel of Fig. 4. Galaxies fainter than M_B^* at high redshift are significantly less clustered than their counterparts in the present-day Universe, with $r_0 = 2.75 \pm 0.27\ h^{-1}$ Mpc. At the same time, the clustering strength of galaxies brighter than M_B^* is comparable to that observed locally with a correlation length up to $r_0 = 4.77 \pm 0.61\ h^{-1}$ Mpc. We therefore observe that at redshift $z \simeq 0.9$, as luminosity increases above L^*, the clustering length suddenly rises to values comparable to those observed locally for galaxies with similar $M_B - M^*$.

4.2. The correlation function slope γ

As we show in Fig. 5, the dependence of the correlation function slope γ on the galaxy intrinsic luminosity in the high-redshift sample differs strongly from the local measurements. Locally, γ has a remarkably constant value, with $\gamma \simeq 1.7$ measured both by the much larger local surveys and – in a very

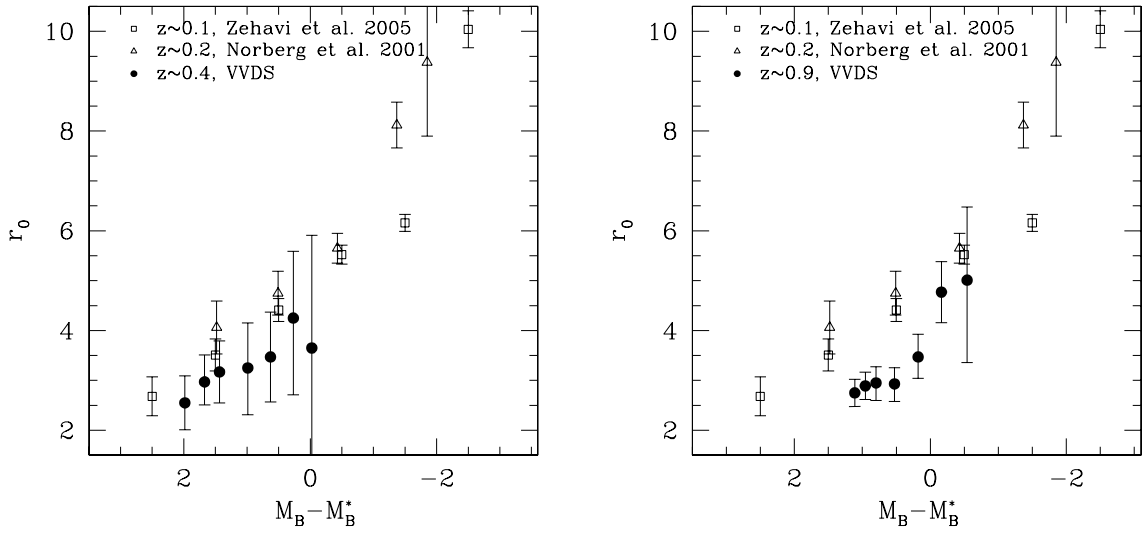

Fig. 4. *Left panel*: dependence of the clustering length r_0 on the median luminosity of galaxies in the local Universe from 2dFGRS and SDSS compared to the VVDS measurements at $z \sim 0.4$. *Right panel*: the same local reference values from 2dFGRS and SDSS compared to the VVDS measurements at $\langle z \rangle \sim 0.9$.

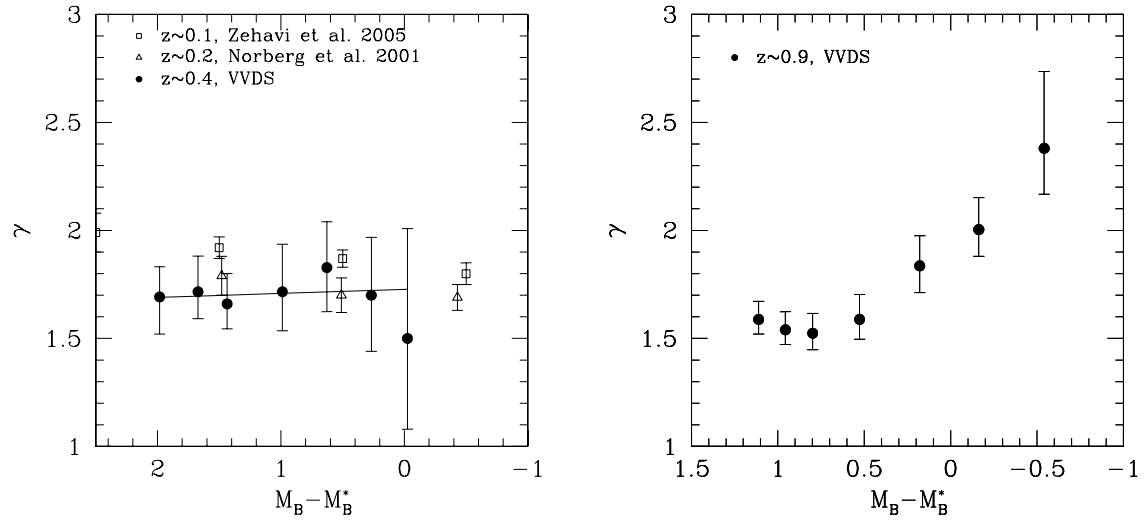

Fig. 5. Measured values of the slope of $\xi(r)$, γ, as a function of the median luminosity of galaxies at low redshift (*left panel*) and at $z \sim 0.9$ (*right panel*). While locally and up to $z \sim 0.5$ γ remains practically constant (with the best rms fit $\gamma = 1.73 - 0.02(M_B - M_B^*)$, marked as a solid line), in the distant Universe it shows a clear scaling with luminosity for galaxies brighter than $M_B^* + 0.5$: the spatial correlation function becomes steeper for galaxies of increasing luminosity.

consistent way – by VVDS in our closer redhift bin $z \sim 0.4$. Conversely, at high z, $\xi(r)$ clearly steepens with increasing luminosity for all sub-samples brighter than $M_B \simeq M_B^* + 0.5$. We find that for $M_B - M_B^* > 0.5$, the slope of the correlation function is consistent with $\gamma = 1.55 \pm 0.08$, while for $M_B - M_B^* < 0$ the slope goes up to $\gamma = 2.38^{+0.36}_{-0.21}$.

4.3. The relative bias of different luminosity classes

To interpret our results and to compare them to local surveys, we compute the relative bias parameter, b/b^*, which gives the amplitude of the correlation function relative to that of L^* galaxies. Consistently with the 2dFGRS analysis (e.g. Norberg et al. 2002) we define the relative bias of the generic ith sample with a given median luminosity L, with respect to that corresponding to L^*, as

$$\frac{b_i}{b^*} = \sqrt{\frac{\left(r_0^i\right)^{\gamma_i}}{\left(r_0^*\right)^{\gamma^*}}} r^{\gamma^* - \gamma^i}, \tag{4}$$

and estimate it at the fixed $r = 1\ h^{-1}$ Mpc scale (see also Meneux et al. 2006, for a slightly different definition).

To apply this formula to the low-redshift samples, we need to estimate the values of r_0 and γ for M_B^* galaxies, that we obtain by a linear fit to the observed VVDS data in the left panel of Fig. 4 (avoiding the very uncertain value measured at M_B^*). We then plot the corresponding values of b/b^* for our samples in Fig. 6. In this figure we also plot the 2dFGRS and SDSS data, together with the analytic fitting relations provided for them,

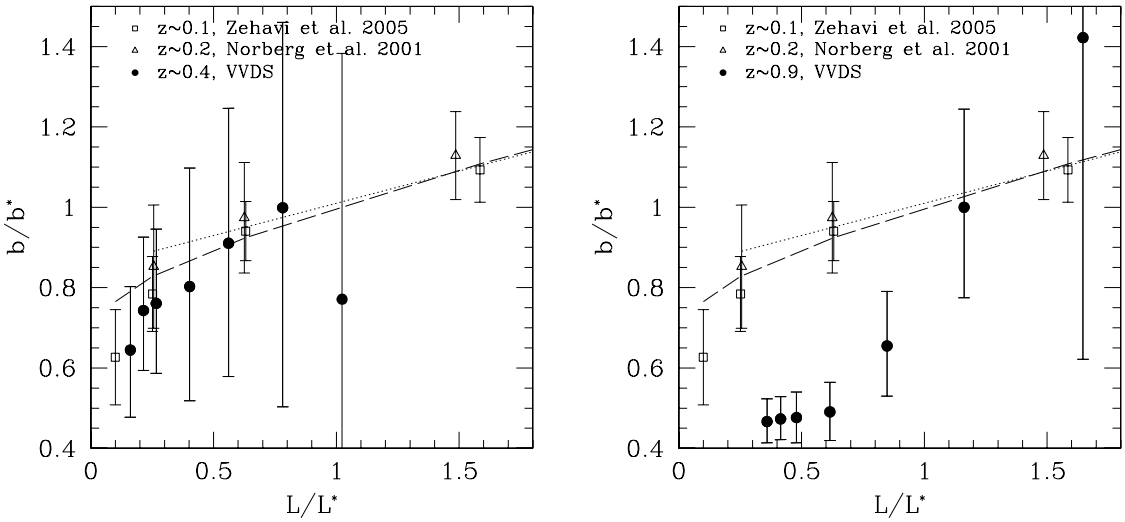

Fig. 6. The variation of the relative bias in the VVDS sub-samples (filled circles) as a function of luminosity using the clustering of L^* galaxies as a reference point, compared to the 2dFGRS (open triangles) and SDSS (open squares) local results. The dashed and dotted lines show, respectively, the best fits made for the SDDS and 2dFGRS measurements.

$b/b^* = 0.85 + 0.16L/L^*$ for the 2dFGRS (Norberg et al. 2002) and $b/b^* = 0.85 + 0.15L/L^* - 0.04(M - M^*)$ for the SDSS (Tegmark et al. 2004). Given the error bars, we can say that the low-redshift VVDS results are in good agreement with both the SDSS and the 2dFGRS fits.

In the high-redshift samples the situation is clearly different. As we can see from the right panel of Fig. 6, the value of b/b^* rises steeply from low values $b/b* \simeq 0.5$ at low luminosities to values that, statistically, are consistent with those of the local samples for $L > L^*$ galaxies, $b/b* \simeq 1 - 1.4$. At the same time the difference on relative bias between of galaxies fainter and brighter than L^* becomes very large. This appears to be an indication that going back in time the bias contrast of luminous galaxies to the rest of the population becomes stronger and is consistent with the fact that fainter galaxies are found to be significantly less biased tracers of the mass than the L^* galaxies even at this relatively high redshift (Marinoni et al. 2005).

5. Summary and discussion

The projected correlation functions that we have measured from our set of volume limited sub-samples of the VVDS are in general fairly well fitted by a single power-law in the range $0.1 \leq r/h^{-1}\mathrm{Mpc} \leq 10$, both for the low-redshift and high-redshift samples. This allows us to use variations in r_0 and γ to characterize the global dependence of clustering on luminosity at high redshift and compare it to similar low-redshift results. The observed behaviour has strong implications for HOD models, as it directly impacts on any recipe for populating dark matter halos at high redshift. Deviations from the power-law shape, although extremely interesting for constraining HOD models (e.g. Zehavi et al. 2005) are not analyzed in this paper and will be the subject of future work.

We observe that for median redshifts $z \simeq 0.9$ ($0.5 < z < 1.2$) the clustering length has a low, nearly constant value $r_0 \simeq 2.9\, h^{-1}$ Mpc for luminosities $M_B < M_B^*$, rising suddenly for $M_B > M_B^*$ and approaching values $r_0 \simeq 5\, h^{-1}$ Mpc similar to those of local galaxies with comparable luminosity (relatively to the characteristic value M_B^*, Norberg et al. 2001). This behaviour is consistent with general predictions by hierarchical models of galaxy formation (Benson et al. 2001), where luminous galaxies are more confined to the peaks of the large-scale density field, going back in redshift, simply due to the higher bias of the parent halos.

Another important result of this work is the clear detection of a systematic steepening of the high-redshift correlation function for absolute magnitudes brighter than $\sim M_B^* + 0.5$ (Fig. 5). This kind of behaviour is in general not seen either in our closer $z \sim 0.4$ sample or in the large local surveys, although Zehavi et al. (2005) do detect an increase of γ in their most luminous volume-selected sample. A similar trend with increasing (UV) luminosity has been recently observed for a population of Ly-break galaxies at $z \geq 4$ in the Subaru Deep Field (Kashikawa et al. 2005). These authors are able to reproduce their observed relationship with a HOD model in which they introduce multiple LBGs into massive dark matter haloes. This amplifies the clustering strength at small scales, steepening the correlation function. A similar interpretation could be applied to our data. Finally, the observed relative bias of galaxies at high redshift provides evidence for a clear difference in the clustering properties of galaxies fainter or brighter than the characteristic luminosity: sub-samples with $M_B \lesssim M_B^*$ behave in a way that is very similar to local samples while the relative bias of samples with $M_B \gtrsim M_B^*$ remains significantly lower.

Results presented in this paper show that there is a significant redshift evolution of the luminosity dependence of both the normalization and slope parameter of the galaxy correlation function. This specific observation can provide an important test of galaxy formation models, constraining in particular the multiplicity of luminous galaxies within massive halos at $z = 1$.

Note added in proof In a parallel paper Coil et al. (2006) perform a similar measurement at $z \sim 1$ using the DEEP-2 survey. Although they explore a narrower range in median luminosities, they also detect

a first hint of the steepening of $w_p(r_p)$ above M_B^* and a rise of the correlation length with luminosity. Considering cosmic variance and the different selection function (unlike the VVDS, DEEP-2 is not a purely magnitude-limited survey), the overall results from these two data sets are thus in good agreement.

Acknowledgements. We thank Peder Norberg for very useful comments and suggestions.
This research has been developed within the framework of the VVDS consortium.
This work has been partially supported by the CNRS-INSU and its Programme National de Cosmologie (France), and by Italian Ministry (MIUR) grants COFIN2000 (MM02037133) and COFIN2003 (num.2003020150).
The VLT-VIMOS observations have been carried out on guaranteed time (GTO) allocated by the European Southern Observatory (ESO) to the VIRMOS consortium, under a contractual agreement between the Centre National de la Recherche Scientifique of France, heading a consortium of French and Italian institutes, and ESO, to design, manufacture and test the VIMOS instrument.

References

Abazajian, K., Zheng, Z., Zehavi, I., et al. 2005, ApJ, 625, 613
Benoist, C., Maurogordato, S., Da Costa, L. N., Cappi, A., & Schaeffer, R. 1996, ApJ, 472, 452
Benson, A. J., Cole, S., Frenk, C. S., Baugh, C. M., & Lacey, C. G. 2001, MNRAS, 327, 1041
Berlind, A. A., Weinberg, D. H., Benson, A. J., et al. 2003, ApJ, 593, 1
Blaizot, J., Wadadekar, Y., Guiderdoni, B., et al. 2005, MNRAS, 360, 159
van den Bosch, F. C., Yang, X., & Mo, H. J. 2003, MNRAS, 340, 771
Coil, A. L., Newman, J. A., Cooper, M. C., et al. 2006, ApJ, submitted [arXiv:astro-ph/0512233]
Cooray, A., & Sheth, R. 2002, Phys. Rept., 372, 1
McCracken, H. J., Radovich, M., Bertin, E., et al. 2003, A&A, 410, 17
Davis, M., & Peebles, P. J. E. 1983, ApJ, 267, 456
Davis, M., Meiksin, A., Strauss, M. A., da Costa, L. N., & Amos, Y. 1988, ApJ, 333, L9
Franzetti, P., & the VVDS team 2005, in preparation
Gao, L., Springel, V., & White, S. D. M. 2004, MNRAS, 363, 66
Guzzo, L., Iovino, A., Chincarini, G., Giovanelli, R., & Haynes, M. P. 1991, ApJ, 382, L5
Guzzo, L., Bartelett, J. G., Cappi, A., et al. 2000, A&A, 355, 1
Hamilton, A. J. S. 1988, ApJ, 331, L59
Harker, G., Cole, S., Helly, J., et al. 2005, MNRAS, submitted [arXiv:astro-ph/0510488]
Ilbert, O., Tresse, L., Zucca, E., et al. 2005, A&A, 439, 863
Iovino, A., Giovanelli, R., Haynes, M., Chincarini, G., & Guzzo, L. 1993, MNRAS, 265, 21
Jing, Y. P., Börner, G., & Suto, Y. 2002, ApJ, 564, 15
Jing, Y. P., Mo, H. J., & Boerner, G. 1998, ApJ, 494, 1
Kaiser, N. 1984, ApJ, 284, L9
Kashikawa, N., Yoshida, M., Shimasaku, K., et al. 2005, ApJ, in press [arXiv:astro-ph/0509564]
Kauffmann, G., Nusser, A., & Steinmetz, M. 1997, MNRAS, 286, 795
Kravtsov, A. V., Berlind, A. A., Wechsler, et al. 2004, ApJ, 609, 35
Landy, S. D., & Szalay, A. S. 1993, ApJ, 412, 64
Le Fèvre, O., Saisse, M., Mancini, D., et al. 2003, SPIE, 4841, 1670
Le Fèvre, O., Mellier, Y., McCracken, H. J., et al. 2004, A&A, 417, 839
Le Fèvre, O., Vettolani, G., Garilli, B., et al. 2005b, A&A, 439, 845
Le Fèvre, O., Guzzo, L., Meneux, B., et al. 2005a, A&A, 439, 877
Marinoni, C., Le Fèvre, O., Meneux, B., et al. 2005, A&A, 442, 801
Marinoni, C., & Hudson, M. J. 2002, ApJ, 569, 101
Maurogordato, S., & Lachieze-Rey, M. 1991, ApJ, 369, 30
Meneux, B. 2005, Ph.D. Thesis, Université de Provence
Meneux, B., Le Fèvre, O., Guzzo, L., et al. 2005, A&A, submitted [arXiv:astro-ph/0511656]
Mo, H. J., & White, S. D. M. 1996, MNRAS, 282, 347
Norberg, P., Baugh, C. M., Hawkins, E., et al. 2001, MNRAS, 328, 64
Norberg, P., Baugh, C. M., Haekins, E., et al. 2002, MNRAS, 332, 827
Peacock, J. A., & Smith, R. E. 2000, MNRAS, 318, 1144
Pollo, A., Meneux, A., Guzzo, L., et al. 2005, A&A, 439, 887
Seljak, U. 2000, MNRAS, 318, 203
Sheth, R. K., & Tormen, G. 1999, MNRAS, 308, 119
Sheth, R. K., & Tormen, G. 2004, MNRAS, 350, 138
Tegmark, M., Blanton, M. R., Strauss, M. A., et al. 2004, ApJ, 606, 702
Valls-Gabaud, D., Alimi, J.-M., & Blanchard, A. 1989, Nature, 341, 215
White, S. D. M., Davis, M., Efstathiou, G., & Frenk, C. S. 1987, Nature, 330, 351
Willmer, C. N. A., Da Costa, L. N., & Pellegrini, P. S. 1998, ApJ, 115, 869
Zehavi, I., Weinberg, D. H., Zheng, Z., et al. 2004, ApJ, 608, 16
Zehavi, I., Zheng, Z., Weinberg, D. H., et al. 2005, ApJ, 630, 1

[1] Laboratoire d'Astropysique de Marseile, UMR 6110 CNRS, Université de Provence, BP 8, 13376 Marseille Cedex 12, France
e-mail: agnieszka.pollo@oamp.fr
[2] INAF – Osservatorio Astronomico di Brera, via Bianchi 46, 23807, Merate & via Brera 28, 20121 Milano, Italy
[3] INAF – Osservatorio Astronomico di Bologna, via Ranzani 1, 40127 Bologna, Italy
[4] INAF – IASF Milano, via Bassini 15, 20133 Milano, Italy
[5] Institut d'Astrophysique de Paris, UMR 7095, 98 bis Bvd Arago, 75014 Paris, France
[6] Observatoire de Paris, LERMA, 61 Avenue de l'Observatoire, 75014 Paris, France
[7] Centre de Physique Théorique CNRS – Luminy and Université de Provence, UMR 6207, 13288 Marseille Cedex 9, France
[8] Laboratoire d'Astrophysique de l'Observatoire Midi-Pyrénées (UMR 5572), 14 avenue E. Belin, 31400 Toulouse, France
[9] INAF – Osservatorio Astronomico di Roma, via di Frascati 33, 00040 Monte Porzio Catone, Italy
[10] INAF – IRA, via Gobetti 101, 40129 Bologna, Italy
[11] Max Planck Institut fur Astrophysik, 85741 Garching, Germany
[12] School of Physics & Astronomy, University of Nottingham, University Park, Nottingham, NG72RD, UK
[13] Universitat Postdam, Astrophysik, 14469 Postdam, Germany
[14] Università di Bologna, Dipartimento di Astronomia, via Ranzani 1, 40127 Bologna, Italy
[15] Astronomical Observatory, Jagiellonian University, ul. Orla 171, 30-244 Kraków, Poland
[16] Imperial College London, South Kensington Campus, London SW7 2AZ, UK
[17] INAF – Osservatorio Astronomico di Capodimonte, via Moiariello 16, 80131 Napoli, Italy
[18] Universitá di Milano-Bicocca, Dipartimento di Fisica, Piazza delle Scienze 3, 20126 Milano, Italy
[19] Integral Science Data Centre, ch. d'Écogia 16, 1290 Versoix, Switzerland
[20] Geneva Observatory, ch. des Maillettes 51, 1290 Sauverny, Switherland